THE JOURNAL OF PHYSICAL CHEMISTRY B

Article

pubs.acs.org/JPCB

Structure and Topology of Soda-Lime Silicate Glasses: Implications for Window Glass

O. Laurent, B. Mantisi, and M. Micoulaut*

Laboratoire de Physique Théorique de la Matière Condensée, Paris Sorbonne Universités UPMC, Boite 121, 4, Place Jussieu, 75252 Paris Cedex 05, France

ABSTRACT: The structural and topological properties of soda-lime silicate glasses of the form $(1-2x)SiO_2-xNa_2O-xCaO$ are studied from classical molecular dynamics using a Buckingham type potential. Focus is made on three compositions (x = 6%, 12%, and 18%) which are either silica-rich or modifier-rich. We compare the results to available experimental measurements on structural properties and find that the simulated pair correlation function and total structure factor agree very well with available experimental measurements from neutron diffraction. The detail of the structural analysis shows that the Na and Ca coordination numbers tend to evolve with composition, and with increasing modifier content, changing from 5.0 to 5.6 and from 4.0 to 5.0 for Ca and Na, respectively. The analysis from topological constraints shows that the picture derived on a heuristic basis using classical valence rules remains partially valid. Ultimately, typical elastic phases are identified from the application of rigidity theory, and results indicate that the 6% system is stressed-rigid, whereas the modifier-rich composition (18%) is flexible. These results receive support from a full analysis of the vibrational density of states showing the low-energy bands at E < 20 meV increase as the system becomes flexible, providing another indirect signature of the presence of rigid to flexible transitions in this archetypal glass. Consequences for window glass are discussed under this perspective.

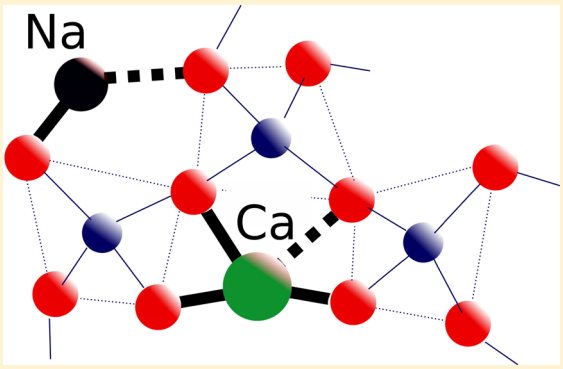

I. INTRODUCTION

Soda-lime silicates not only form an interesting class of basic network glasses but also represent the archetypal base material for various domestic, industrial, and commercial applications in glass science,[1] including the well-known example of window glass, or promising bioactive materials for bone medical implants.[2] Applications usually result from an appropriate alloying of additives into the base glass and lead to specific properties that are continuously optimized. However, many of these additives are strongly influenced by the properties of the underlying soda-lime silicate compound which affects transport properties, such as diffusion or viscosity, or thermal properties, such as density or thermal expansion. Ultimately, these properties depend on the underlying network structure and the way this structure evolves with composition. The description of structural properties of soda-lime glasses appears, thus, to be a fundamental issue in glass science with, obviously, a high degree of possible applications that could emerge from an increased understanding.

Surprisingly, there have not been many structural studies on this system in the literature, although the interest in this ternary system is quite old[3] and has been focused in early reports on the practical issue of immiscibility[4,5] and liquid-phase separation.[6] The structure of soda-lime glasses of chemical formula $n_S SiO_2-n_N Na_2O-n_C CaO$ (termed $n_S-n_N-n_C$ hereafter) has been investigated from X-ray,[7,8] and neutron diffraction,[8,9] and there is indication that both modifiers (Na_2O and CaO) disrupt the base silica network by creating nonbridging oxygens (NBOs) in the immediate vicinity of the cations. These cations fill the voids left in the structure and have between four and six oxygen neighbors. In the continuous random network picture,[10,11] it is furthermore assumed that the cations have a random distribution. However, there is recent evidence that in soda-lime glasses Ca and Na are nonrandomly distributed,[12] a result that seems in line with the proposition that silica-rich and cation-rich regions (i.e., channels[13]) coexist in the structure. Such heterogeneous distributions have been detected in the related Na and Ca binary systems from diffraction[14,15] and molecular dynamics (MD) simulations.[16,17]

A recent theoretical effort has been published by Cormier et al.[8] using both MD and reverse Monte Carlo (RMC) modeling, and by Karlsson et al. using RMC alone.[9] Tilocca and de Leeuw have performed an analysis on a single composition in the ternary compound (75−10−15) from first-principles MD using the Car−Parrinello approach,[18] quenched from a classical MD with a force field derived by Teter.[19] Given the small relaxation times, the structure was found to be very close to the one obtained from an independent study[20] on $75SiO_2-(25-x)Na_2O-xCaO$. To the best of our knowledge, the latter represents the only systematic numerical study of soda-lime

Received: June 20, 2014
Revised: October 1, 2014
Published: October 8, 2014

dx.doi.org/10.1021/jp506155p | J. Phys. Chem. B 2014, 118, 12750−12762

glasses as a function of composition. Results showed that both Ca and Na play a network modifying role but that the first coordination shell of the cations was found to be better defined for the Ca atoms. Weak changes in structure were obtained as a function of composition. An additional structural investigation has been reported by Tilocca and co-workers[21] using different interatomic potentials for the ternary (75−10−15) silicate, and the structural results from model potentials (shell models) were compared to a reference calculation using *ab initio* simulations.

An alternative framework for extended studies in composition relies on rigidity theory[22−24] which focuses on the key microscopic physics while filtering out all possible atomic-scale details which represent a burden for the computational effort and prevent a thorough investigation of compositional trends. The approach is based on the concepts which are directly derived from the Maxwell elasticity theory for macroscopic structures.[25,26] In fact, from a mechanical viewpoint, the bond-stretching (BS) and bond-bending (BB) interactions which constrain a glass network at a molecular level can be identified[22] with mechanical constraints n_c which are compared to the available degrees of freedom n_d (3 in 3D). At the exact boundary $n_c = n_d$ corresponding to the isostatic stability criterion defined by Maxwell,[26] a flexible to rigid transition has been predicted,[23,24] verified from various observed anomalies in materials properties.[27,28]

A pioneering application of rigidity theory on soda-lime glasses is due to Kerner and Phillips[29,30] who showed that a combination of the isostatic criterion ($n_c = 3$) and the requirement that the average size of small-ring structures is 6 (such as for the low-pressure forms of silica polymorphs), leads to an *ideal* composition of 74−16−10. It is quite remarkable that such simple and elegant conditions have led to a composition that is very close to the one corresponding to window glass. In the related binaries of soda-lime glasses (SiO_2−Na_2O and SiO_2−CaO), effects of rigidity have been also detected. In the former, it has been shown[31,32] that a rigid to flexible transition occurs at composition of ≃20% Na_2O modifier, and an intermediate phase[27] has been obtained between 18% and 22% soda. In the latter, Raman integrated intensities of tetrahedral modes[33] which are typical of the local structure of silica (Q^4 motifs), exhibit an abrupt decrease at ≃45% CaO and indicate the breakdown of the stressed-rigid network structure. This trend is consistent with an increase of ionic conduction[34] which is promoted because low-energy deformation (floppy) modes typical of flexible networks ($n_c <$ 3) facilitate the creation of doorways for ions and enhance mobility.[35] Building on these concepts from rigidity theory, Gupta and Mauro have extended the theory to account for temperature-dependent constraints[36] and have successfully predicted from simple structural models mechanical, thermal, and structural properties of multicomponent silicate glasses[37,38] using CaO or Na_2O or B_2O_3 as additives.

There is a major drawback in the rigidity approach, however. In the search for ideal glasses or *optimal* compositions that are isostatic or stress-free ($n_c = 3$) and may have potentialities for interesting applications, constraint counting rules are often established on an empirical or heuristic basis.[29,36] Recently, it has been shown that constraint counting can be applied with confidence when coupled to realistic atomic-scale trajectories from molecular simulations.[39−41] This allows one to access in a neat way an exact count of bond-stretching and bond-bending forces constraining the network at the molecular level, as exemplified in sodium silicates[39] and silica[40] and in different chalcogenides.[41,42] Here we build on this approach and investigate three compositions of soda-lime silicates using MD simulations. We find that the structure in real space is dominated by the base network structure of silica for all compositions. However, as the modifier content is increased, new structural correlations emerge, and these are mostly driven by the increased contribution of Na−O and Ca−O pairs. The modifier-poor glass is found to exhibit increased Ca−Ca correlations, while Na−Na typical distances are substantially decreased. The analysis of the topology reveals that Na and Ca have between four and five neighbors, respectively. However, it is found that such neighbors lead only to BS constraints that strongly depend on the neighbor rank, unlike the oxygen neighbors of Si that define the $SiO_{4/2}$ tetrahedron. There are virtually no contributions in terms of BB constraints. The global count of constraints n_c allows then identifying a flexible to rigid transition for the ternary compound. Taken together, these results reveal that modifier-rich soda-lime glasses are flexible and display deformation (floppy) modes that bear similarities with weakly connected glasses,[27] whereas, on the opposite end, silica-rich compositions are stressed-rigid. This feature may eventually induce the observed phase separation[5] in the liquid phase, as also observed in chalcogenide glasses.[43]

This work is organized as follows. In section II, we provide the simulation details and describe the structural properties in section III. We then apply MD-derived constraint counting algorithms to the three investigated compositions in section IV and discuss the findings in section V. Finally, section VI draws some conclusions and summarizes the findings.

II. SIMULATION METHODOLOGY

Three systems of 3,000 atoms have been simulated at different compositions according to previous investigations of soda-lime silicates using rigidity theory.[29] Indeed, we have selected in the wide range of possible compositions $(1-x-y)SiO_2-xNa_2O-yCaO$ the join representing $x = y$ (red curve in Figure 1) which crosses the predicted[29] isostatic stability line $n_c = 3$. We have selected a silica-rich (88−6−6), a modifier-rich (64−18−18), and an additional system (76−12−12). According to ref 29, the

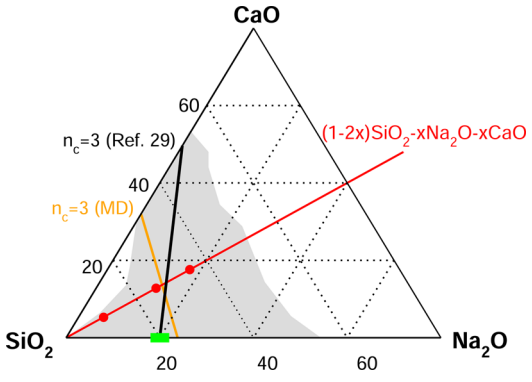

Figure 1. Compositional triangle of soda-lime silicates. The gray zone indicates the reported glass-forming range,[44] and the black line, the anticipated Maxwell stability line[29] fulfilling $n_c = 3$. The orange curve is the isostatic line determined from the present MD simulations (see section IV.C). Red dots correspond to the present investigated compositions from MD simulations. The green bar in the binary sodium silicate system corresponds to the reported intermediate phase.[31,32]

dx.doi.org/10.1021/jp506155p | J. Phys. Chem. B 2014, 118, 12750−12762

first two compositions are supposed to represent a stressed-rigid and a flexible network, respectively.

The interaction potential used in the present study is a two-body potential of Buckingham type which has been fitted by Xiang and Du[45] (parameters can be found in the relevant reference). It contains an attractive dispersive term in $1/r^6$, a Coulombic term, and a repulsive part. We have also added a strongly repulsive part to prevent any collapse of the system at high temperatures. This repulsive part has been switched off at a lower temperature (3,000 K), and results on liquid structures at $T \leq 3{,}000$ K with or without the correction did not show any significant differences.

Molecular dynamics simulations (DLPOLY[46]) were carried out in the (N,P,T) ensemble at zero pressure using a leapfrog Verlet algorithm with a time step of 2 fs. Typical runs were about 2 ns. We first homogenized the systems at a temperature of 5,000 K before accumulating trajectories (1−2 ns) by steps of 500 K down to 300 K. Averages were performed over 2 ns. Figure 2 shows a typical obtained structure for the 64−18−18

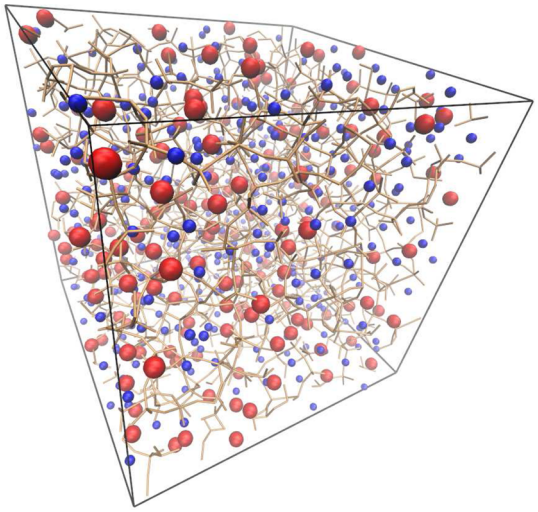

Figure 2. Snapshot of the modifier-rich composition 64−18−18 of a soda-lime silicate. Red and blue spheres represent the calcium and sodium atoms, respectively. The network backbone (Si,O) is represented by simple bars.

system. To check for possible system size effects, we have also investigated two systems of 81,000 and 24,000 atoms for the 88−6−6 and 76−12−12 glasses, respectively. Again, the structure functions (pair correlation functions and structure factor) did not show any significant changes, thus providing confidence that the 3,000 atoms size is sufficient to investigate structural and topological properties. This is also in line with a recent size-effect study using first-principles molecular dynamics simulations.[47]

III. STRUCTURAL PROPERTIES

At zero pressure, the calculated densities are found to be in good agreement with experimental measurements for close compositions; we found 2.41, 2.49, and 2.59 g·cm^{-3} with decreasing silica content, i.e. for 88−6−6, 76−12−12, and 64−18−18. This can be compared with measurements for the close compositions 90−6−4, 78−12−10, and 66−18−16 which have densities of 2.310, 2.455, and 2.595 g·cm^{-3}, respectively.[44]

A. Global Structure. Figure 3 shows the total pair correlation function, calculated from the partial ones using

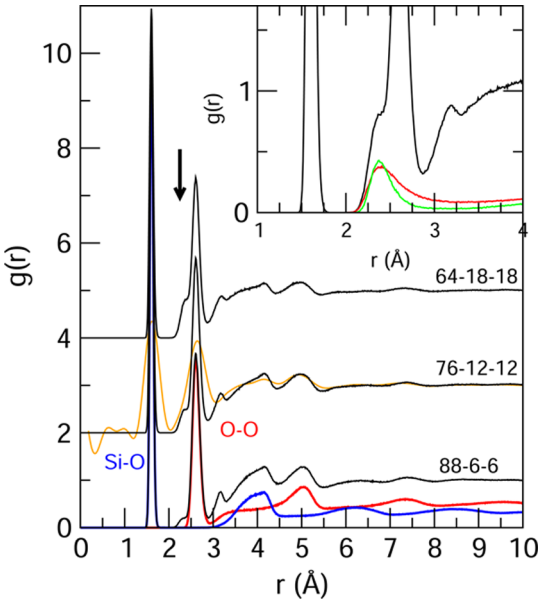

Figure 3. Total calculated pair correlation function $g(r)$ of soda-lime glasses for different compositions. The blue and the red curves for the 88−6−6 composition represent the contribution from Si−O and O−O, respectively. Experimental data[8] on a close system (75−15−10) are shown (orange curve). The arrow indicates the shoulder peak described in the text. The inset shows the function $g(r)$ of the modifier-rich composition (64−18−18, same as the main panel) and the contributions from Na−O (red) and Ca−O (green) correlations. See text for details.

$$g(r) = \frac{\sum_{i,j} c_i c_j b_i b_j g_{ij}(r)}{\left(\sum_i c_i b_i\right)^2} \quad (1)$$

where c_i represents the concentration of species i and b_i are the neutron coherence lengths.

We first remark that our calculated pair correlation function of the 76−12−12 is very close to the experimental neutron pair correlation function[8] for a slightly different composition (75−15−10), all typical distances being recovered from the simulation. We note that, similar to many other numerical works,[20,39] the simulation leads to a glass network that is much more structured, and this leads to much more intense first peaks (1.61 and 2.61 Å) for the function $g(r)$. However, this should not affect the topological constraint count detailed in later text given that the structuration mostly affects the Si−O and O−O correlations (blue and red curves in Figure 3) which define the tetrahedra. In silicates, corresponding silicon and oxygen constraints are indeed always intact because they define the rigid network backbone. Furthermore, topological constraints focus only on nearest-neighbor interactions (stretching and bending) so that typical second-neighbor correlations, i.e., those leading to typical distances between 3 and 5.5 Å, will only weakly impact the results.

Similarly, we find that the calculated structure factor $S(k)$ also reasonably well reproduces the structure for the composition 76−12−12, i.e., the one that is the closest to a soda-lime composition studied experimentally (75−10−15) by Cormier et al.[8] from neutron diffraction (Figure 4). All typical features are reproduced, i.e., the principal peak at ≃5.5 Å^{-1} and the peaks at either low (1.5 and 3.0 Å^{-1}) or high wavevector (8.0 and 11.5 Å^{-1}). At the lowest modified silicate composition (88−6−6), the structure factor appears to be very close to the

dx.doi.org/10.1021/jp506155p | J. Phys. Chem. B 2014, 118, 12750−12762

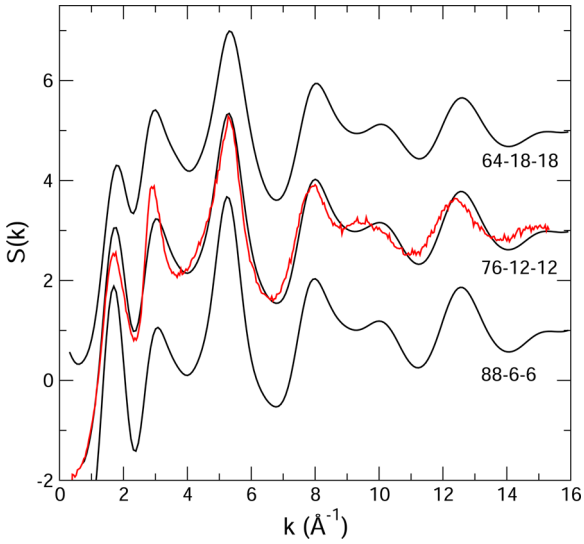

Figure 4. Total calculated structure factor $S(k)$ of soda-lime glasses for different compositions. Experimental data[8] on a close system (75−15−10) are shown (red curve).

one obtained for vitreous silica,[48] i.e., with dominant contributions at 2.0, 3.0, and 5.5 Å^{-1}. With increasing modifier content, however, the principal peak tends to broaden and the difference between the first two peaks at low wavevector decreases. The addition of network-modifying cations also leads to a decrease of the intensity of the first sharp diffraction peak, as also previously observed for binary alkali silicates.[49]

In real space, one can notice that at short distances all functions $g(r)$ are dominated by the contributions arising from both Si−O and O−O correlations which lead to marked peaks at ≃1.61 Å (the Si−O bond distance, from the blue curve $g_{SiO}(r)$ in Figure 3) and at ≃2.61 Å (the O−O bond distance, red curve $g_{OO}(r)$), i.e., distances which are found to be nearly identical to those found in the base silica glass[48] or in sodium silicates.[39] This simply indicates that the local tetrahedral geometry is maintained for the three compositions of interest, given that neither the edges of the tetrahedra (i.e., the distance d_{O-O}) nor the tetrahedral parameter[50] $\delta = d_{Si-O}/d_{O-O}$ changes with composition. For an ideal tetrahedron, one has indeed $\delta = (3/8)^{1/2} = 0.612$, and here it is found $\delta \simeq 0.61(5)$ for all investigated systems.

Given the dominant contribution of both Si−O and O−O correlations, the global shape of $g(r)$ does not vary much with composition. However, a shoulder peak of the O−O main peak builds up at ≃2.37 Å with an increase of modifier content. This peak arises from the increase of Na−O (red curve in the inset of Figure 3) and Ca−O correlations (green curve) as one moves from the 88−6−6 to the modifier-rich 64−18−18 alloy.

The detail of the relevant partial pair correlation functions $g_{ij}(r)$ is shown in Figure 5 and allows determination of the typical distances involved in the network and the way these evolve with modifier content. The partials Si−Si, Si−O, and O−O do not exhibit any significant change (not shown), and we focus here on Na- and Ca-based partials. It is found (Figure 5) that changes mostly occur between the modifier-rich 64−18−18 and the other compositions, and these changes manifest by an important reduction of the intensity of the principal peak in $g_{NaO}(r)$ and $g_{CaO}(r)$ found at 2.40 and 2.36 Å, respectively. Note that the Na−O distance found in this ternary is very close to the one found in the related binary sodium silicate.[39] More

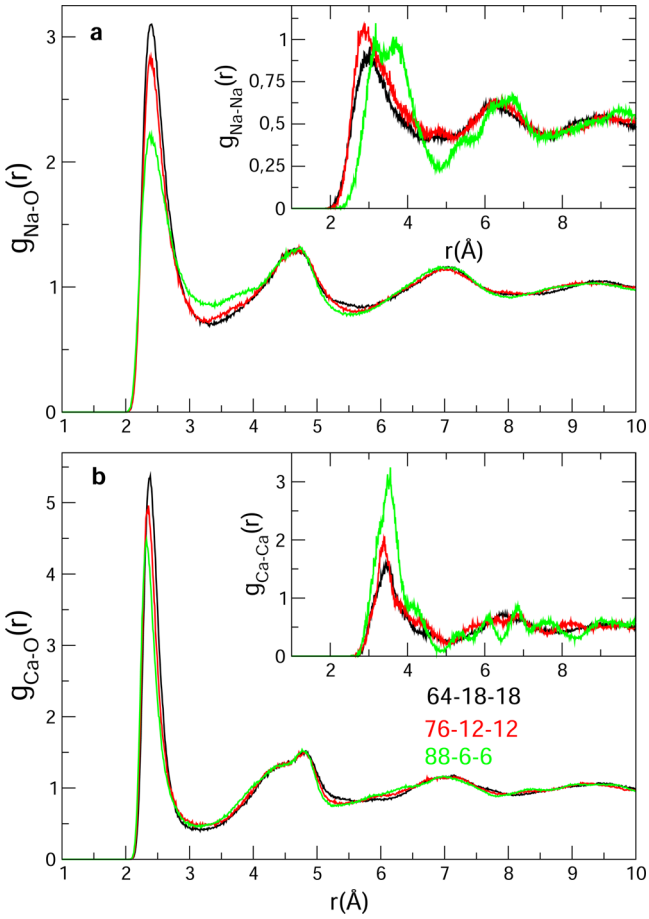

Figure 5. Partial pair correlation function $g_{NaO}(r)$ (a), g_{CaO} (b), and $g_{NaNa}(r)$, g_{CaCa} for soda-lime silicate glasses with composition 88−6−6 (red), 76−12−12 (black), and 64−18−18 (green). The minimum r_{min} of $g_{NaO}(r)$ is indicated with an arrow.

important changes take place in Ca−Ca and Na−Na correlations (insets of Figure 5). In the $g_{NaNa}(r)$ function, the addition of modifiers leads to a decrease of the first peak distance (≃3.5 Å for 88−6−6), and the peak furthermore appears to be bimodal with typical distances found at 3.2 and 3.7 Å. Similarly, the intensity of the main peak of the Ca−Ca correlation function (inset of Figure 5b) decreases in the 64−18−18 glass, indicating that more Ca−Ca correlations occur as the modifier content of glass is steadily increased.

The results on the typical distances can be directly compared to reference data obtained from *ab initio* Car−Parrinello (CP) simulations (specifically Table 10 of ref 21) or shell-model MD calculations of a slightly different composition $75SiO_2$−$10Na_2O$−15CaO. We find that all our obtained interatomic distances lie in the range of these different models. The obtained Na−O and Ca−O distances for the 76−12−12 compound (2.38 and 2.36 Å, respectively) are indeed close to the CP calculations of 2.35 and 2.30 Å, respectively. Similarly the Ca−Ca distance (d_{CaCa} = 3.44 Å) is also found to be in the range of values determined from these different structural models with 3.32 Å ≤ d_{CaCa} ≤ 3.5 Å. We finally note that the composition affects the Na−Na correlations as noticed from the inset of Figure 5a. As a result, for the 76−12−12 glass we determine from the pair correlation function $g_{NaNa}(r)$ a distance of d_{NaNa} = 3.01 Å which is lower than the calculated[21] range of distances 3.3 ≤ d_{NaNa} ≤ 3.5 Å. However, as noticed from the

dx.doi.org/10.1021/jp506155p | J. Phys. Chem. B 2014, 118, 12750−12762

inset of Figure 5a, the silica-rich system (88−6−6) contains correlation distances which are larger (3.5 Å), suggesting a strong effect due to composition.

B. BO and NBO Correlations. As previously reported,[39] for the oxygen correlations we can also use an alternative framework using the oxygen differentiation which makes the distinction between the bridging oxygens (BO) connecting two $SiO_{4/2}$ tetrahedra and those which are found in the vicinity of the (Na,Ca) cations, usually termed[20] as NBOs. To determine the BOs, we check that such oxygen atoms have as first neighbors two silicon atoms. We find a fraction η of BO atoms of $\eta = 1 - \alpha = 87.1\%$, 72.5%, and 55.7% for the 88−6−6, 76−12−12, and 64−18−18 glasses, respectively. Here, α represents the fraction of NBO atoms. Classical valence rules suggest that each addition of a Ca (respectively Na) atom should lead to the creation of two (respectively one) NBOs, and from the stoichiometry $(1-2x)SiO_2-xNa_2O-xCaO$ the fraction η of BOs should therefore evolve as $(1 - 3x)/(1 - x)$. This leads to the values 87.2%, 72.7%, and 56.1% for the 88−6−6, 76−12−12, and 64−18−18 glasses, and which are very close to those determined from the numerical trajectories.

Figure 6 shows NBO- and modifier-centered pair correlation functions, and the former has been split into contributions related to Na and to Ca ions (broken and solid lines in panel a). One recovers the first peak distance at 1.61 Å corresponding to the Si−NBO bond distance. Interestingly, $g_{NBO}(r)$ exhibits a second peak consisting of a double contribution at 2.34 and 2.61 Å (Figure 6a). The latter is associated with NBO−oxygen correlations that can be also detected from the partial correlation function $g_{OO}(r)$ (Figure 3), whereas the former is associated with NBO−modifier distances. This becomes apparent when the peak at 2.34 Å in $g_{NBO}(r)$ is compared to the $g_{Na}(r)$ and $g_{Ca}(r)$ partials (Figure 6b,c), which have their main (first) peak at this same distance of 2.34 Å. One can thus conclude that the NBO−(Ca,Na) is longer than the NBO−Si distance but shorter than the NBO−oxygen bond distance. As the temperature is increased to 2,000 K, we finally note a global broadening of all correlating distances (peaks) in $g_{NBO}(r)$, attributed to the increased diffusion of the alkali cations which cancels to some extent the structural correlations of the cations.

C. Coordination Numbers. From the obtained simulated pair correlation functions (Figure 5), we obtain by integrating up to corresponding first minima r_{min} the partial coordination numbers for the different compositions, using

$$n_{ij} = 4\pi\rho \int_0^{r_{min}} r^2 g_{ij}(r)\, dr \qquad (2)$$

where ρ is the system density.

We find that for all compositions, one has $n_{SiO} = 4$ and $n_{BO} = 2$. The Na coordination is equal to 3.95, 4.62, and 5.03 for the 88−6−6, 76−12−12, and 64−18−18 glasses, respectively. The Ca coordination is equal to 5.02, 5.35, and 5.55 for the 88−6−6, 76−12−12, and 64−18−18 glasses, respectively. These results are recovered when the neighbor distributions are calculated, and, in fact, one finds that for, e.g., the calcium atoms ($n_{Ca} = 5.35$), the minimum r_{min} coincides with distances at which the fifth and the sixth neighbor distribution functions dominate (blue curves in Figure 6b,c for the 64−18−18 glass).

Results indicate that an increase in modifier composition leads to an increase of both n_{Ca} and n_{Na}, and the origin can be determined from an inspection of corresponding partial pair correlations (Figure 5). For Ca (Figure 5b), an increase of the modifier content leads to a more intense first peak (at 2.35 Å)

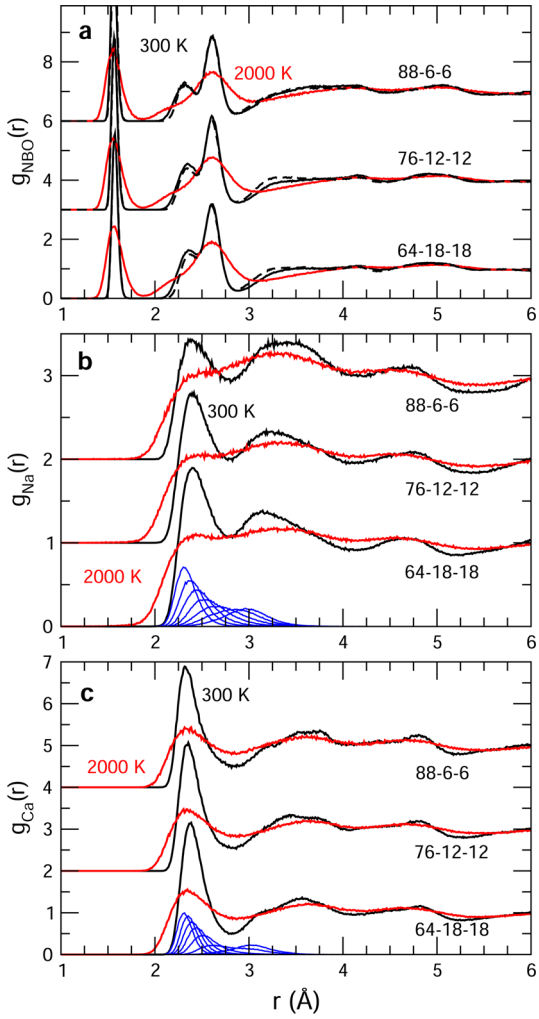

Figure 6. NBO- (a), Na- (b), and Ca-centered (c) partial pair correlation function for the three compositions of interest and two different temperatures (300 K, black; 2,000 K, red). In panel a, the solid and broken lines correspond to NBO−Na and NBO−Ca correlations, respectively. Blue curves in panels b and c correspond to calculated neighbor distributions.

resulting from a better defined neighborhood for the Ca cation for the 68−18−18 composition. For the Na cation (Figure 5a), this effect is also seen, but, in addition, the increase of the modifier content also contributes to a more structured distribution of alkali cations, as evidenced from the more pronounced minimum found at r_{min} in $g_{NaO}(r)$.

IV. TOPOLOGICAL CONSTRAINT COUNTING

In order to link our results to previous investigations on the rigidity of soda-lime silicate glasses,[29,30] we determine topological constraints in the obtained systems by following doublets (pairs, bonds) or triplets (angles) of neighbors over the simulated trajectory. In rigidity theory,[22,23] the dominant interactions which are usually nearest-neighbor bond-stretching (BS) and next-nearest-neighbor bond-bending (BB) forces, and the number of constraints per atom can be exactly computed in a mean-field way, given by

$$n_c = \frac{\sum_{r\geq 2} n_r \left[\frac{r}{2} + 2r - 3\right]}{\sum_{r\geq 2} n_r} \qquad (3)$$

dx.doi.org/10.1021/jp506155p | J. Phys. Chem. B 2014, 118, 12750−12762

where n_r is the concentration of species being r-fold-coordinated. The contribution of the two terms in the numerator is obvious. Each bond is shared by two neighbors, and one has $r/2$ BS bond-stretching constraints for a r-fold atom. For BB (angular) constraints, one notices that a 2-fold atom involves only one angle, and each additional bond needs the definition of two more angles, leading to the estimate of $(2r - 3)$. For 1-fold terminal atoms, a special count[51,52] is achieved as no BB constraints are involved. By defining the network mean coordination number $\overline{r}$ of the network by

$$\overline{r} = \frac{\sum_{r\geq 2} r n_r}{\sum_{r\geq 2} n_r} \tag{4}$$

one can reduce eq 3 to the simple equation:

$$n_c = \frac{\overline{r}}{2} + 2\overline{r} - 3 \tag{5}$$

and the application of the Maxwell stability criterion ($n_c = 3$) leads to the predicted isostatic composition of $\overline{r} = 2.40$ in 3D,[23] and anomalies are found, indeed, in a large number of covalent glasses.[27,28]

As mentioned earlier,[31,32] given the ionic nature of the chemical bonding in silicates, the weaker interactions involving cations (Na and Ca) cannot be treated straightforwardly using eq 3, and one can now rely on the MD-generated trajectories to extract the number of constraints, similarly to a recent application on a selected composition of the SiO_2–Na_2O binary.[39] In fact, if two atoms (or three atoms defining an angle) remain neighbors over the simulation time, then their motion can be considered as being correlated, and a topological constraint is identified from the doublet (respectively triplet for an angle). On the contrary if such atoms separate from each other at some point during the simulation and are no longer first neighbors, then the corresponding constraint can be considered as broken and should not contribute to the rigidity of the network. Recombinations of bonds or angles are of course possible, but these aspects are obviously driven by the bond lifetime. In the glass, given the very large bond lifetime of the network-forming ions (Si,O), an intact constraint can be considered as being intact over the whole trajectory,[39] consistent with the simple two-state model proposed by Mauro and Gupta.[36]

To put the analysis in measurable quantities, one extracts from the radial (angular) motion of such doublets (triplets) a pair (angular) distribution which is characterized by a first moment (i.e., a mean) and a second moment (i.e., a standard deviation) σ_i with $i = r$ or $i = \theta$ depending on the considered situation, bonds or angles. It quantifies the excursion around the mean value and provides information about the strength of the underlying bond-stretching (bond-bending) interaction.[39−41] If the radial (angular) excursion is small, one will identify a corresponding topological constraint (Figure 7); otherwise the constraint is considered as broken and does not contribute to rigidity. We now apply these concepts and algorithms to the case of the soda-lime silicates.

A. Radial Constraints. The number of first neighbors have been previously determined from the integration of the partial pair correlation functions and have led, e.g., to $r_{Si} = 4.02$, $r_O = 2.01$, $r_{Ca} = 5.35$, and $r_{Na} = 4.62$ for the 76−12−12 compound. An analysis of the radial excursions (Figure 8) shows that not all neighbors give rise to mechanically effective BS constraints. In fact, while the silicon atoms have a number n_c^{BS} that is exactly

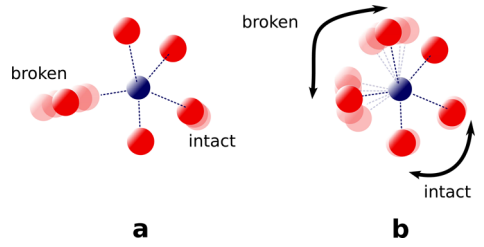

Figure 7. Schematic method of constraint counting from MD-generated configurations. Large (small) radial (a) or angular (b) excursions around a mean value are characterized by large (small) standard deviations on radial or angular distributions, representing broken (intact) constraints.

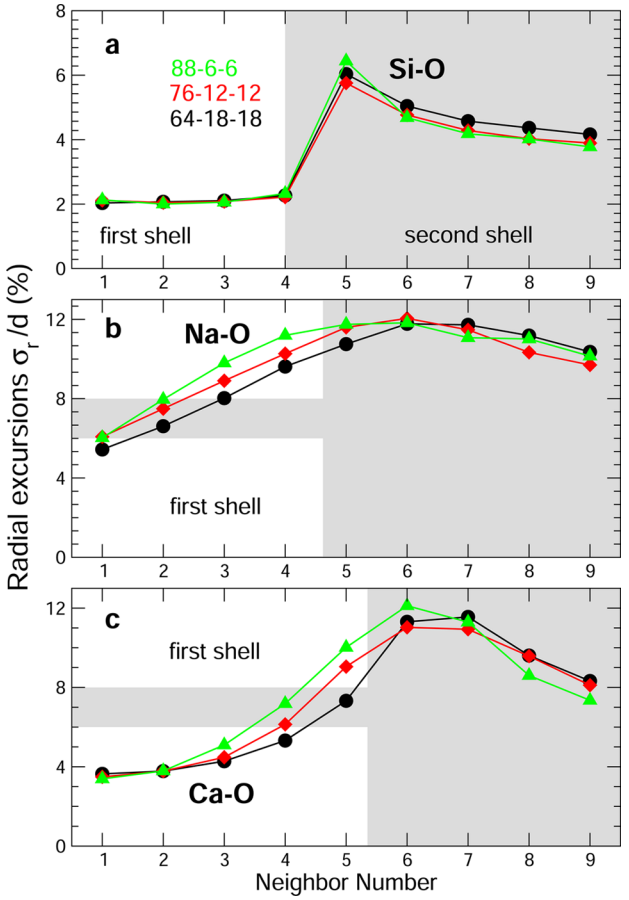

Figure 8. (a) Si−O, (b) Na−O, and (c) Ca−O radial standard deviations σ_r/d as a function of neighbor number for the three compositions of interest. Here d is the peak position of the relevant neighbor distributions. The shaded areas correspond either to the second shell of neighbors, which is nonrelevant for constraint counting, or to the approximate limit ($7 \pm 1\%$) between intact (low σ_r) or broken (large σ_r) bond-stretching constraints. The limit between the first and the second shell of neighbors is the one of the 76−12−12 compound (4.62 and 5.35 for Na and Ca, respectively).

equal to $r_{Si}/2$ because of a well-separated gap between the neighbor $N_n = 4$ and $N_n = 5$ (Figure 8a), the cations have a value σ_r/d that depends on the rank of the neighbors (Figure 8b,c). Here d is the peak position (first moment) of the relevant neighbor distributions. Radial excursions do indeed increase with N_n. An approximate limit for broken and intact constraints can be set around $\sigma_r/d \simeq 7\%$, close to what has been reported previously,[39] which is also fairly close to the well-

dx.doi.org/10.1021/jp506155p | J. Phys. Chem. B 2014, 118, 12750−12762

known Lindemann criterion[53,54] stating that atomic motion occurs when the root-mean-square displacement $\langle r^2 \rangle^{1/2}$ is about 10% of the nearest bond distance.

Parts b and c of Figure 8 show the same calculation for the alkali cations, and using this threshold limit of 7%, we note that between one and two sodium BS constraints and between three and four calcium BS constraints are active in the relevant (first) shell of coordination. We furthermore note that, in contrast with the silicon BS analysis, there is an effect due to the chemical composition, as modifier-rich soda-lime silicates tend to reduce radial excursions for the cations.

There is an alternative way to determine the BS constraints. Over the simulation trajectory, we follow a given distance between two selected atoms. For each individual atom k, the radial motion over the time trajectory leads indeed to a single bond distance distribution $P_k(r)$ characterized by mean $\langle r_k \rangle$ (the first moment of the distribution), and a second moment (or standard deviation σ_{rk}). The latter represents, once again, a measure of the strength of the underlying BS interaction, this time acting on an individual atom, and not system-averaged as represented in Figure 8. In fact, if σ_{rk} is large, it suggests that the BS restoring force which maintains the bond distance fixed around its mean value $\langle r_k \rangle$ is ineffective. As a result, the corresponding BS topological constraint will be broken and will not contribute to network rigidity. The opposite reasoning can be applied for low values of σ_{rk} which will give rise to an intact BS constraint and contribute to n_c. The average over the whole system then leads to a distribution $f(\sigma_r)$ of standard deviations which can be analyzed.

Figure 9 shows such distributions $f(\sigma_r)$ for selected species and a given composition. It is seen that the distributions are

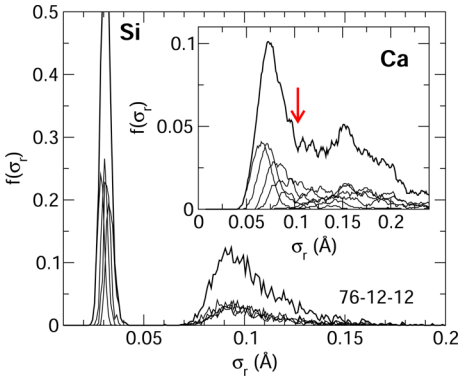

Figure 9. Radial second moments distribution of the Si and Ca (inset) for the 76−12−12 glass. The red arrow indicates the minimum of the distribution separating intact BS constraints from broken ones.[39]

essentially bimodal and contain a low-σ_r part which corresponds to intact BS constraints and a high-σ_r part associated with broken ones. With increasing temperature, the whole distribution shifts to higher values in σ_r and the lower σ_r contribution collapses. This simply reveals that thermal activation breaks the BS and BB constraints.[40]

For well-defined environments (Si atoms), the gap between the fourth (at σ_r = 0.03 Å) and the fifth bond distribution (at σ_r = 0.08 Å) is well-defined and signals without any ambiguity that one has, in fact, n_c^{BS}(Si) = 4 per bond. For the cations (e.g., Ca atoms, inset of Figure 9), we determine the number of constraints by calculating the density of the distribution at the minimum of $f(\sigma_r)$. This leads to n_c^{BS}(Ca) = 3.2 for the 76−12−12 glass, a value that is close to the one determined from the criterion of 7% (Figure 8). We also find n_c^{BS}(Na) = 1.3 for this compositions of 76−12−12, and additional numbers are provided in Table I.

Table I. Calculated Number of Constraints, BS and BB Contributions in Soda-Lime Glasses, Using Either the Lindemann Criterion (Figure 8) or a Cutoff from the Radial Standard Deviation Distributions $f(\sigma)$ (Figure 9)

	88−6−6	76−12−12	64−18−18
N_c^{BS}(Si)	2	2	2
N_c^{BB}(Si)	5	5	5
N_c^{BS}(BO)	$(1-\alpha)$	$(1-\alpha)$	$(1-\alpha)$
N_c^{BB}(BO)	$(1-\alpha)$	$(1-\alpha)$	$(1-\alpha)$
N_c^{BS}(NBO)	$\alpha/2$	$\alpha/2$	$\alpha/2$
Lindemann (Figure 8)			
N_c^{BS}(Ca)	3	4	4
N_c^{BS}(Na)	1	1	1
N_c	3.33	3.03	2.75
σ distributions (Figure 9)			
N_c^{BS}(Ca)	3.4	3.2	3.2
N_c^{BS}(Na)	1.6	1.8	1.8
N_c	3.39	3.10	2.80

B. Angular Constraints. In a similar way we can segregate rigid (intact) and flexible (broken) angles through a second moment analysis of typical bond angle distributions, following a method introduced in ref 39. to enumerate angles that contribute to rigidity.

We select around a central atom of type A N neighbors which define $\mathcal{N}_A = N(N-1)/2$ bond angles and lead to partial bond angle distributions (PBADs) $P_A(\theta)$ once averages are performed over simulation time and system. From this analysis, one realizes that only a limited number of angles will be well-defined (Figure 10) and will lead to a second moment

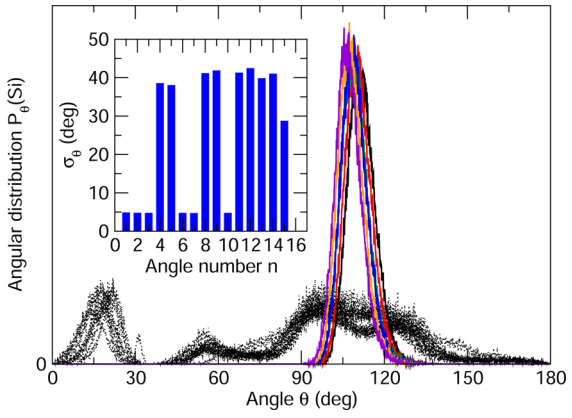

Figure 10. Angles around a silicon atom, defined by the N = 6 first neighbors leading to $\mathcal{N}_a$ = 15 possible partial bond angle distributions $P_{Si}(\theta)$. Colored curves correspond to PBADs having a low standard deviation σ_θ (inset, blue bars). See text for details.

σ_θ which is small. For the case of Si-centered bond angles (A = Si), six angles are rigid given that they have $\sigma_\theta \leq 5°$ (inset of Figure 10). These define the tetrahedra, and corresponding PBADs are, indeed, centered at the tetrahedral angle of 109°. Details of other applications can be found in refs 39−42.

The same analysis can then be performed for all species including BOs and NBOs, and corresponding results are

dx.doi.org/10.1021/jp506155p | J. Phys. Chem. B 2014, 118, 12750−12762

displayed in Figure 11. It can be noticed that only BO and Si atoms contribute to BB rigidity, with one and five constraints,

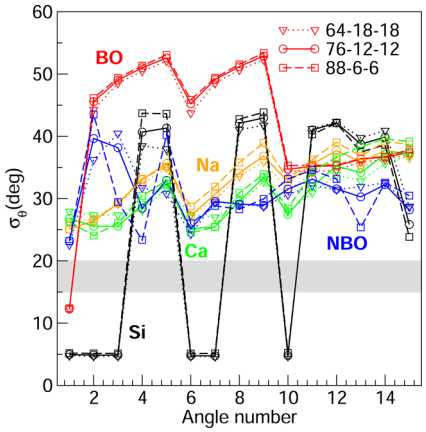

Figure 11. Second moments σ_θ of the species-dependent (Si, BO, NBO, Na, Ca) PBADs as a function of arbitrary angle number (here $\mathcal{N}_a$ = 15). for the three glasses of interest.

respectively. Note that, for the case of Si atoms, six standard deviations with a low σ_θ are obtained (Figure 10) but only five angles are independent given that the sixth angle can be determined from the five other ones. On the opposite, it now becomes clear that Ca- and Na-centered bond angle distributions are wide and have no directional bondings, because $\sigma_\theta \simeq 30°$ for all angles around both cations, and indicate large angular excursions. As a result, all possible BB constraints associated with Na and Ca can be considered as broken.

Once again, the coupling between realistic numerical models and constraint counting reveals that a clear distinction has to be made between coordination numbers calculated from the integration of the partial pair correlation functions $g_{ij}(r)$ and coordination numbers that lead to effective mechanical constraints, as determined from Figures 8 and 11. Obviously, a direct application of eq 3 using coordination numbers from eq 2 will lead to incorrect results.

C. Total Number of Constraints. Having established the number of constraints and the population α of NBO atoms, we then use eq 3 to determine the total number of constraints n_c per atom for the three compositions of interest. For the Si atoms, we find seven constraints (five BB and two BS) as in other Group IV oxides or chalcogenides.[42] We similarly find for the population of BOs (having a fraction $1 - \alpha$) two constraints (one BB and one BS). NBOs only contribute to half of a constraint. Ca and Na atoms contribute only to BS constraints (Figure 8).

The number of constraints per atom is then given by

$$n_c = \frac{11 - 18x - 3\alpha(1 - x) + x[n_c^{BS}(Ca) + 2n_c^{BS}(Na)]}{3 - x} \quad (6)$$

and since we have checked that the MD determined population of BO atoms was following the one calculated from a classical valence rule, $\eta = (1 - 3x)/(1 - x) = 1 - \alpha$, one may write

$$n_c = \frac{11 - 24x + x[n_c^{BS}(Ca) + 2n_c^{BS}(Na)]}{3 - x} \quad (7)$$

Corresponding results are given in Table I using either the 7% threshold value or the cutoff (minimum value) in the distribution $f(\sigma_r)$. These show that the silica-rich composition (88−6−6) is stressed-rigid (3.33−3.39) as it has n_c larger than the value of 3, whereas the modifier-rich composition is flexible with n_c found between 2.75 and 2.80. The additional composition 76−12−12 is nearly isostatically rigid (3.03−3.10).

Using these constraints, we can check if the rigid to flexible transitions in the corresponding binaries can be recovered. For the $(1-x)SiO_2-xNa_2O$ glass, a simple use of eq 3 and the numbers of Table I leads to a mean-field threshold composition at

$$x_c = \frac{1}{6 - n_c^{BS}(Na)} \quad (8)$$

leading to a threshold between x_c = 20 and 24% that is consistent with the observation of the intermediate phase (18−22%) in the binary sodium silicates.[31,32] For the calcium silicate binary $(1-x)SiO_2-xCaO$, we similarly find

$$x_c = \frac{2}{9 - n_c^{BS}(Ca)} \quad (9)$$

and using $n_c^{BS}(Ca) = 4$, we find a threshold at around 40%, somewhat smaller than the experimental one,[33,34] this threshold depending on the choice of $n_c^{BS}(Ca)$. In the ternary soda-lime silicate, along the considered line $(1-2x)SiO_2-xNa_2O-xCaO$, we obtain an isostatic condition (n_c = 3) for the composition:

$$x_c = \frac{2}{21 - 2n_c^{BS}(Na) - n_c^{BS}(Ca)} \quad (10)$$

which leads (using Table I) to a threshold at x_c = 14.1% which marks the onset of a flexible network as the modifier content is increased.

Finally, for a more general ternary soda-lime silicate of the form $(1-x-y)SiO_2-xNa_2O-yCaO$, we derive the number of constraints:

$$n_c = \frac{11 - 12x - 12y + yn_c^{BS}(Ca) + 2xn_c^{BS}(Na)}{3 - y} \quad (11)$$

and a Maxwell stability condition (n_c = 3) can be established:

$$2 = 2x[6 - n_c^{BS}(Na)] + y[9 - n_c^{BS}(Ca)] \quad (12)$$

which leads for the values $n_c^{BS}(Ca)$ = 3.2 and $n_c^{BS}(Na)$ = 1.8 to an approximate isostatic line (orange line) represented in Figure 1, and which differs from the one established by Kerner and Phillips,[29] as discussed in later text.

V. DISCUSSION

Having in hand the results of topological constraints from MD simulations combined with algorithms based on radial and angular excursions, and the possible stiffening of the network structure as the silica content is increased, we first focus on the vibrational properties before discussing the much broader consequences that emerge from our findings.

A. Vibrational Density of States. In order to detect if there are floppy modes which are typical of flexible networks, we have calculated the vibrational density of states (VDOS) $g(\omega)$ using the Fourier transform of the velocity−velocity autocorrelation function:

dx.doi.org/10.1021/jp506155p | J. Phys. Chem. B 2014, 118, 12750−12762

$$g(\omega) = \frac{1}{Nk_BT} \sum_{j=1}^{N} \int_{-\infty}^{\infty} \langle \mathbf{v}_j(t)\, \mathbf{v}_j(0) \rangle\, e^{i\omega t}\, dt \quad (13)$$

In parallel, we have performed the calculation of the eigenvalues of the dynamical matrix, following a procedure previously applied to silica glasses[55] or to jammed solids,[56,57] and this also leads to a frequency histogram that corresponds to the density of vibrational states. It should be reminded that eq 13 gives the VDOS spectrum from a statistical point of view using linear response theory and can be mathematically derived for liquids.[58] It uses the time evolution of the particles, lists the derivative of displacement with respect to time, and correlates velocities in time. The Fourier transform then gives typical vibrations of the system, but using this method does not permit one to access the nature of the modes. On the other hand, the dynamical matrix method computes and diagonalizes the second derivative of the Hessian, defined by

$$H_{ij} = \frac{\partial^2 V(r)}{\partial \mathbf{r}_i\, \partial \mathbf{r}_j} \quad (14)$$

where $V(r)$ is the interaction potential.[45] The eigenmodes are the vibrational modes of the system associated with their frequencies which are the eigenfrequencies of the matrix. One can directly visualize the modes using this method, but the diagonalization can be a complex process depending on the size of the system and the range of the interactions; the longer the interactions, the lesser sparse is the matrix which will lead to an enhanced difficulty in diagonalization. The VDOS corresponds then to the number of modes having a frequency between ω and $\omega + d\omega$; it can thus be directly computed using this definition. For smaller systems such as the one presented here (3,000 atoms), the statistics using eq 13 can be more accurate, since one deals with a set of several configurations in time, whereas the diagonalization of eq 14 performs a statistics over the number of modes present in the system, i.e., $3N - 3$ to describe the whole spectrum.

In Figure 12, we represent the VDOS for the three compositions of interest using either eq 13 or eq 14. For the silica-rich one (88−6−6), we can eventually compare to the reported experimental spectrum of silica[48] and a simulated one using a model reported in ref 55. using eq 14. It is seen that the main features of the VDOS of the 88−6−6 compound consist in a broad band between 0 and 20 THz (83 meV), a second band made of a peak at 32 THz (132 meV), and a secondary peak at 37 THz (153 meV). When compared to the silica spectra, we note that the high-frequency band remains nearly unchanged, and it is also unchanged with respect to simulated spectra of amorphous silica,[59] except the red shift. Furthermore, the broad band between 0 and 20 THz, also found in simulated SiO_2 ($x = 0$), is not detected in the experimental spectrum which shows a dominant contribution at 12 THz. The evolution with composition is characterized by a stiffening of the high-frequency band that leads to a global shift of the VDOS toward higher frequencies, as the system becomes flexible.

The broad bands between 15 and 25 THz seem to be correlated to two typical peaks in Raman scattering at 600 and 800 cm^{-1}, whereas the peak at 30 THz gives rise to the main peak[60,61] found at 1,200 cm^{-1} for a close composition (72−15−8). These features are usually associated with Q^n species stretching vibrations[62,63] where n represents the number of BO atoms on a Si tetrahedron. Bands at 450−560 cm^{-1} are

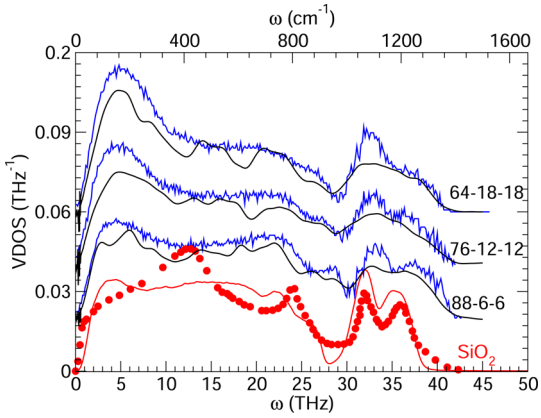

Figure 12. Calculated vibrational density of states (VDOS) in soda-lime silicate glasses for select compositions: black curves using the velocity autocorrelation function (eq 13) and blue curves using the eigenvalues of the dynamical matrix (eq 14). The experimental reference spectra for amorphous silica ($x = 0$) is shown for reference (red circles), and a calculation of the density of vibrational states using velocity autocorrelation functions of a model silica (red curve[55]) is also shown. The energy scale (cm^{-1}) is provided (top axis) for the connection with the Raman spectra (see text for details).

attributed to Si−O−Si symmetric stretching modes in Q^4 (the base $SiO_{4/2}$ tetrahedra) and Q^3 species (a tetrahedra with one NBO), while the main band at 1,100 cm^{-1} is associated with Si−O stretching modes of Si tetrahedra having NBOs. From our simulated VDOS, we now notice that the intensity of the band at 1,100 cm^{-1} increases, in fact, as a function of modifier. This result is consistent with the fact that the corresponding Raman band is driven by the NBOs, and that their population is growing with modifier content.

B. Identification of Floppy Modes. The structure of the low-frequency band changes in an important fashion with composition. This band nearly reduces, indeed, to a prominent peak at 5 THz whose intensity grows with modifier content, and underscores important partial contributions from O anions (Figure 13). For the flexible composition 64−18−18, the VDOS does not contain any vibrational modes with zero frequency (floppy modes) as first suggested by Thorpe[23] and Cai and Thorpe[64] from idealized bond-depleted amorphous networks. These findings also contrast with those reported on densified silica networks where the $SiO_{4/2}$ tetrahedra are taken as rigid[65] and which lead to a gap at $\omega \simeq 0$ for stressed-rigid networks. In the present system, the results are actually much closer to what has been observed experimentally on different chalcogenide glasses;[66] i.e., one does not have $g(\omega) \neq 0$ at $\omega \simeq 0$ in flexible glasses which would indicate the presence of zero energy modes. One reason for the absence of such modes comes from the fact that residual forces are not taken into account in the rigidity approach[23] (dihedral, van der Waals, and so on), and these lead to a finite value for the floppy mode energy,[66] of about 5 meV, clearly observed from the experimental VDOS of elemental Se. In the case of silica, the contribution of such weak interactions, typically van der Waals and BO bending interactions, can be estimated to a similar value using the calculated stiffness[67] of the Si−O−Si bending interaction, and the molecular mass to form a frequency of 1.4 THz (5.8 meV).

The detail of the contributions to the total VDOS (Figure 13) shows that the spectrum is dominated by the oxygen atoms, this statement being valid for all compositions. Silicon atoms

dx.doi.org/10.1021/jp506155p | J. Phys. Chem. B 2014, 118, 12750−12762

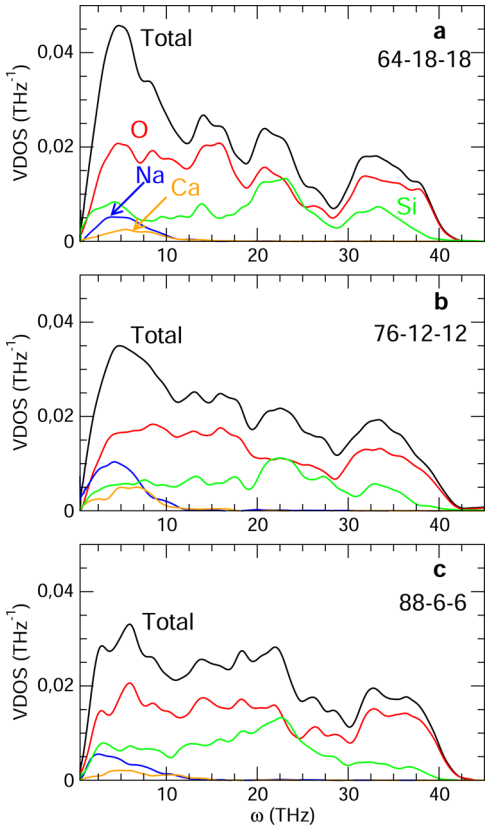

Figure 13. Calculated partial vibrational density of states in soda-lime silicate glasses for select compositions: total (black curve, same as Figure 12, and contributions from oxygen (red), silicon (green), calcium (orange), and sodium (blue).

contribute essentially to the bands between 20 and 40 THz. Finally, the cations (Ca, Na) lead to typical vibrations that are located in the low-frequency band between 0 and 10 THz. These features are actually quite close to those determined for similar glasses such as sodium silicates.[68]

To track the effect of rigidity and floppy modes, we now focus on the low-frequency region of the VDOS. Since various contributions are involved in this frequency range, and since weak interactions also contribute, we represent in Figure 14

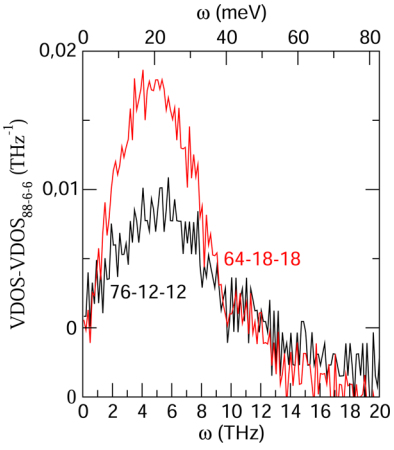

Figure 14. Difference spectra between the calculated VDOS (dynamical matrix) of the 64−18−18 (red) and 76−12−12 (black) glasses and the VDOS of the stressed-rigid composition (88−6−6).

difference spectra representing the VDOS of the 76−12−12 and 64−18−18 compounds minus the reference compound 88−6−6. The latter has been found to be stressed-rigid (Table I) and, for this reason, should not contain any floppy modes and may serve as a reference system in order to remove all other possible low energy contributions arising from the network-forming species such as silicon and oxygen. It is found that as the modifier content increases, a contribution at 5 THz (20 meV) builds up, which has been previously assigned to oxygen vibrations (Figure 13). This frequency also appears to correspond to the floppy mode frequency determined both in chalcogenide[66] glasses and silica.[56] We can, thus, conclude that the onset of flexibility leads to increased deformation modes that are associated with vibrations/local deformations involving an oxygen motion. This contribution to the difference VDOS is certainly not negligible because the amplitude is about 0.01−0.02 THz^{-1} (Figure 14), i.e., about 50% of the total spectrum.

C. Comparison with the Kerner−Phillips Model. The present findings can also be compared to the model of Kerner and Phillips establishing the number of constraints n_c for a soda-lime glass of the form $(1-x-y)SiO_2-xNa_2O-yCaO$. While Si and BO are counted according to the classical valence (octet) rule, it is assumed that even the modifier cations are loosely bonded to more than one oxygen ion so that one can generalize Pauling's idea of resonating bonds to include resonating bond constraints. This leads to a count of fractional constraints for resonating alkali modifiers that follow a classical valence rule; i.e., it assumed that $n_{Ca} = 2$ and $n_{Na} = 1$, leading to $n_c^{BS}(Ca) = 1$ and $n_c^{BB}(Ca) = 1$, and $n_c^{BS}(Na) = 1/2$ and $n_c^{BB}(Na) = 0$ with the additional condition that bond-bending constraints for sodium are broken because of the nondirectional bonding[51] between the NBO and the Na cation (Figure 15a).

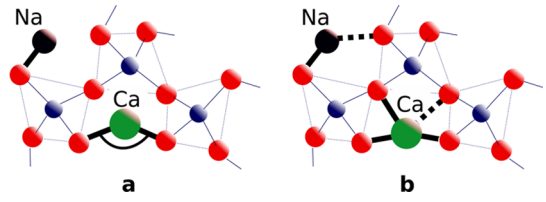

Figure 15. Proposed cation (sodium, black; calcium, green) constraint counting in soda-lime silicates (silicon, blue spheres; oxygen, red spheres): (a) Kerner−Phillips counting based on Pauling's resonant constraints (thick lines) leading to $n_c^{BS}(Na) = 1/2$, $n_c^{BB}(Na) = 0$, $n_c^{BS}(Ca) = 1$, and $n_c^{BB}(Ca) = 1$; (b) MD-based constraint counting (present work) leading to $n_c^{BB} = 0$ for all cations and n_c^{BS}'s larger than those proposed by Kerner and Phillips. Note that neither silicon nor oxygen constraints are represented.

Here, as in ref 29, we find that Si and the BO atoms have, indeed, seven and two constraints, respectively. They arise from $n_c^{BS} = 2$ and $n_c^{BS} = 5$ for the silicon, and $n_c^{BS} = 1$ and $n_c^{BS} = 1$ for the bridging oxygen atom (Table I). The counting differs in the way the cations and the NBO atoms contrain the network (Figure 15b) as it is found from the MD-based counting algorithms that no angular constraints act on theses types of atoms (Figure 11). On the other hand, between three and four stretching constraints are found for the Ca atoms, and between one and two constraints are found for the NBO atom, one of them being related to the Si−NBO bond.

Our obtained picture clearly differs from the one derived from Pauling's resonant constraints,[29] and it is consistent with the computed bond angle distribution $P(\theta)$ showing that the

dx.doi.org/10.1021/jp506155p | J. Phys. Chem. B 2014, 118, 12750−12762

Ca atom can hardly have a single BB constraint[29,30] given the broad distribution $P(\theta)$ for all considered glass compositions (Figure 16). Intact BB constraints usually lead to sharp bond angle distributions such as those displayed in Figure 10 which in turn are characterized by small second moments.[40] Here, the broad distribution shown for the calcium atom, together with the large second moments calculated for this species (Figure 11), leads to the conclusion that one has, indeed, $n_c^{BB} = 0$.

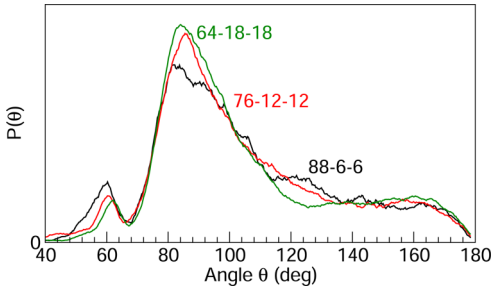

Figure 16. Computed O−Ca−O bond angle distribution for the three select compositions in soda-lime silicate glasses. The small peak at 60° signals edge-sharing Ca polyhedra.[69]

An inspection of Figure 16 furthermore permits one to determine the local geometry of Ca sites. In fact, with a distribution dominated by angles at ≃90°, and a large tail at 140−180°, one identifies an octahedral site geometry for the calcium atoms, consistently with the coordination numbers n_{Ca} = 5.02−5.55 determined in the previous section, which suggests a defective octahedral ordering. This is also close to recent X-ray diffraction results showing the presence of edge-shared Ca polyhedra[69] in a wollastonite ($CaSiO_3$) liquid, and to MD results on the SiO_2−CaO binary glass.[70] However, the calculation of both radial and angular standard deviations reveals that this octahedral geometry is soft given the large angular standard deviations $\sigma_\theta \simeq 25-30°$ (Figure 11) and is mostly defined from the rigid short bonds (2.31−2.45 Å) defining a nearly equatorial plane, and which give rise to the three to four BS constraints. The longer bonds (2.50−2.88 Å) connecting the Ca to the vertices of the octahedra do not contribute to network rigidity, as shown from their larger standard deviation (Figures 8c and 9).

D. Nature of Window Glass. We finally turn to the question of window glass, and having established the constraint count on a firm basis, we may ask what can be the mechanical nature of the typical soda-lime glasses of industrial interest. The question of the chemical composition of window glass has been already questioned nearly a century ago[72] and current applications are determined from the properties under small variations in composition or addition of other various elements (<1%) including Al_2O_3 and K_2O.

A typical float window glass contains 70% SiO_2, 5% MgO, 10% CaO, and 15% Na_2O.[44] Using eq 11 and assuming that one has n_c^{BS}(Ca) = 3.2 and n_c^{BS}(Na) = 1.8, and furthermore assuming at a first stage that Mg atoms act as Ca atoms, we find that the total number of constraints is n_c = 3.05. Similarly, a typical container glass of composition 75%, 10% CaO, and 15% Na_2O leads to n_c = 2.95. Both are found close to the isostatic criterion n_c = 3 which usually leads to a variety of interesting phenomena for glass manufacturers. Isostatic networks lead, indeed, to an enhanced glass-forming tendency or glass stability[74,75] which is revealed by a minimum with composition in the critical cooling rate[76−78] to avoid crystallization or by a maximum[79,80] in the thermal stability $\Delta T = T_x - T_g$, where T_x is the crystallization temperature and T_g the glass transition temperature. Minor corrections can be brought if the coordination number for Mg is taken as being slightly lower than the one of Ca.[73] This will induce a lower contribution of the alkaline earth bond-stretching constraints to eq 11 and shift the isostatic threshold to higher modifier compositions.

Although we must stress that such a mean-field treatment of bonding and rigidity provides only general tendencies, eq 11 contains some interesting information for window glass applications, especially if other joins in the compositional triangle (Figure 1) were to be considered. In the case of Ca/Na substitution along joins of the form SiO_2−(R−x)CaO−$x$$Na_2O$ with arbitrary R and varying x, replacing Na by Ca will lead to an increase of rigidity that can eventually be used for increasing the hardness $\mathcal{H}_v$ of the glasses, given that $\mathcal{H}_v$ scales as $n_c - n_0$, where n_0 is a constant.[37] But at the same time, an increase of rigidity will also lead to melts that tend to segregate or unmix during cooling, a situation that is met for silica-rich compositions.[4] Alternatively, the replacement of Ca by Na induces flexibility that can be used for the enhancement of ionic diffusion[34] or the decrease of viscocity.[61]

VI. CONCLUDING REMARKS

In summary, we have investigated three soda-lime silicate glasses using molecular dynamics simulations and topological constraint counting. The choice of the compositions along the (1−2x)SiO_2−$x$$Na_2O$−$x$CaO join has been motivated by the prediction of a rigid to flexible transition,[29] computed in a mean-field way from the Maxwell isostatic criterion (n_c = 3) and resonant constraints. Here we have used the Xian−Du potential[20] to simulate such glasses using molecular dynamics simulations. We have first successfully compared our structure functions with experimental data that have become available in more recent years.[8] Both pair correlation functions $g(r)$ and structure functions $S(k)$ of the x = 12% glass exhibit, indeed, a very good agreement with the experimental measured functions for a close composition (75SiO_2−15Na_2O−10CaO). This provides confidence that the models are realistic. In a second part, we have then computed the number of topological constraints by analyzing radial and angular excursions which lead to a neat estimate of the number of bond-stretching and bond-bending interactions contributing to rigidity.

We have found that silica-rich networks (88−6−6) are stressed-rigid and are characterized by n_c > 3, whereas modifier-rich soda-lime silicates (64−18−18) are flexible and have n_c = 3.33−3.39. The additional composition (76−12−12) is found to be very close (n_c = 3.03) to the isostatic stability criterion, but the detail of our analysis reveals that the constraint enumeration is different from the one proposed by Kerner and Phillips on a heuristic basis. Here, we find indeed that while Si and BO atoms contribute to seven and two constraints, respectively, Ca and Na cations have only stretching constraints. Furthermore, it is found that the latter depend on the composition, the 88−6−6 exhibiting a smaller number of BS constraints for the Ca atom. Ultimately, a mean-field rigid to flexible transition is detected at a composition of about 14% modifier.

These findings are consistent with a vibrational analysis (VDOS) that permits one to detect that an increased number of low-frequency modes (≃5 THz) are present in the flexible

dx.doi.org/10.1021/jp506155p | J. Phys. Chem. B 2014, 118, 12750−12762

composition (64−18−18). The detail of the analysis permits one, furthermore, to detect that oxygen atoms contribute mostly to these features; i.e., they reveal that at high modifier composition the network contains local deformation modes that are typical of flexible elastic phases.[23] This provides an additional support for our identification of the flexible and stressed-rigid phases.

A few perspectives can be drawn. First, given the predicted presence of a rigid−flexible threshold in soda-lime glasses, one may expect that the corresponding threshold composition will exhibit all of the salient features of isostatic glasses.[27,28] Second, one may not observe a single isostatic composition but rather a finite interval of such isostatic compositions, defining an intermediate phase[81] that is usually revealed by an enthalpic reversibility window from modulated differential scanning measurements. This reversibility window has been already observed in one of the related binaries.[32] We will certainly not speculate further on this issue but will stress at this point that such measurements would be highly desirable. In fact, the identification of an intermediate phase in soda-lime silicates would allow one to design new functionalties, using the properties of isostatic glasses such as thermal stability, space-filling tendency, weak aging as compared to flexible or stressed-rigid glasses, and, finally, enhanced mechanical properties.

AUTHOR INFORMATION

Corresponding Author

*E-mail: mmi@lptl.jussieu.fr. Tel.: +33-147-27-72-40. Fax: +33-147-27-51-00.

Notes

The authors declare no competing financial interest.

ACKNOWLEDGMENTS

O.L. acknowledges financial support from Saint-Gobain Recherche. Discussions with J. C. Phillips, R. Kerner, P. Simon, and P. Boolchand are gratefully acknowledged. We thank L. Cormier for sharing his data on neutron diffraction.

REFERENCES

(1) Mauro, J. C.; Philip, C. S.; Vaughn, D. J.; Pambianchi, M. S. Glass Science in the United States: Current Status and Future Directions. *Int. J. Appl. Glass Sci.* **2014**, *5*, 2−15.
(2) Moawad, H. M. M.; Jain, H. Development of nano-macroporous soda-lime phosphofluorosilicate bioactive glass and glass-ceramics. *J. Mater. Sci.* **2009**, *20*, 1409−1418.
(3) Greig, J. W. Immiscibility in silicate melts: Part II. *Am. J. Sci.* **1927**, *13*, 133−154.
(4) Hammel, J. J. Direct Measurements of Homogeneous Nucleation Rates in a Glass-Forming System. *J. Chem. Phys.* **1967**, *46*, 2234−2244.
(5) Burnett, D. G.; Douglas, R. W. Liquid-liquid phase separation in the soda-lime- silica system. *Phys. Chem. Glasses* **1970**, *11*, 125−135.
(6) James, P. F. Liquid-phase separation in glass-forming systems. *J. Mater. Sci.* **1975**, *10*, 1802−1825.
(7) Warren, B. E.; Biscob, J. Fourier analysis of X-ray patterns of soda-silica glass. *J. Am. Ceram. Soc.* **1938**, *21*, 259−265.
(8) Cormier, L.; Calas, G.; Beneu, B. Structural changes between soda-lime silicate glass and melt. *J. Non-Cryst. Solids* **2011**, *257*, 926−931.
(9) Karlsson, C.; Zanghellini, P.; Swenson, J.; Roling, B.; Bowron, D. T.; Börjesson, L. Structure of alkali alkaline-earth silicate glasses from neutron diffraction and vibrational spectroscopy. *Phys. Rev. B* **2005**, *72*, No. 064206.
(10) Zachariasen, W. H. The atomic arrangement in glass. *J. Am. Ceram. Soc.* **1932**, *54*, 3841−3851.
(11) Wright, A. C.; Thorpe, M. F. Eighty years of random networks. *Phys. Status Solidi B* **2013**, *250*, 931−936.
(12) Lee, S. K.; Stebbins, J. F. Nature of cation mixing and ordering in Na-Ca silicate glasses and melts. *J. Phys. Chem. B* **2003**, *107*, 3141−3148.
(13) Greaves, G. N. EXAFS, glass structure and diffusion. *Philos. Mag. B* **1989**, *60*, 793−800.
(14) Gaskell, P. H.; Eckersley, M. C.; Barnes, A. C.; Chieux, P. Medium-range order in the cation distribution of a calcium silicate glass. *Nature* **1991**, *350*, 675−677.
(15) Mayer, A.; Horbach, J.; Kob, W.; Kargl, F.; Schober, H. Channel Formation and Intermediate Range Order in Sodium Silicate Melts and Glasses. *Phys. Rev. Lett.* **2004**, *93*, No. 027801.
(16) Horbach, J.; Kob, W.; Binder, K. Dynamics of sodium in sodium disilicate: Channel relaxation and sodium diffusion. *Phys. Rev. Lett.* **2002**, *88*, No. 125502.
(17) Jund, P.; Kob, W.; Jullien, R. Channel diffusion of sodium in a silicate glass. *Phys. Rev. B* **2001**, *64*, No. 134303.
(18) Tilocca, A.; de Leeuw, N. H. Structural and electronic properties of modified sodium and soda-lime silicate glasses by Car-Parrinello molecular dynamics. *J. Mater. Chem.* **2006**, *16*, 1950−1955.
(19) Cormack, A. N.; Du, J.; Zeitler, T. R. Alkali ion migration mechanisms in silicate glasses probed by molecular dynamics simulations. *Phys. Chem. Chem. Phys.* **2002**, *4*, 3193−3197.
(20) Cormack, A. N.; Du, J. Molecular dynamics simulations of soda-lime-silicate glasses. *J. Non-Cryst. Solids* **2001**, *293−295*, 283−289.
(21) Tilocca, A.; de Leeuw, N. H.; Cormack, A. N. Shell-model molecular dynamics calculations of modified silicate glasses. *Phys. Rev. B* **2006**, *73*, No. 104209.
(22) Phillips, J. C. Topology of covalent non-crystalline solids I: Short-range order in chalcogenide alloys. *J. Non-Cryst. Solids* **1979**, *34*, 153−181.
(23) Thorpe, M. F. Continuous deformation in random networks. *J. Non-Cryst. Solids* **1983**, *57*, 355−370.
(24) Micoulaut, M.; Phillips, J. C. Rings and rigidity transitions in network glasses. *Phys. Rev. B* **2003**, *67*, No. 104204.
(25) Lagrange, J. L. *Mécanique Analytique*, Paris, 1788.
(26) Maxwell, J. C. On the calculation of the equilibrium and stiffness of frames. *Philos. Mag.* **1864**, *27*, 294−299.
(27) *Rigidity and Boolchand phases in nanomaterials*; Micoulaut, M., Popescu, M., Eds.; INOE Publishing House: Bucarest, Romania, 2009.
(28) *Phase Transitions and Self-Organization in Electronic and Molecular Networks*; Thorpe, M. F., Phillips, J. C., Eds.; Kluwer Academic, Plenum: New York, 2001.
(29) Kerner, R.; Phillips, J. C. Quantitative principles of silicate glass chemistry. *Solid State Commun.* **2000**, *117*, 47−51.
(30) Phillips, J. C.; Kerner, R. Structure and function of window glass and Pyrex. *J. Chem. Phys.* **2008**, *128*, No. 174506.
(31) Vaills, Y.; Qu, T.; Micoulaut, M.; Chaimbault, F.; Boolchand, P. Direct evidence of rigidity loss and self-organization in silicates. *J. Phys.: Condens. Matter* **2005**, *17*, 4889−4896.
(32) Micoulaut, M. Constrained interactions, rigidity, adaptative networks and their role for the description of silicates. *Am. Mineral.* **2008**, *93*, 1732−1748.
(33) Micoulaut, M.; Malki, M.; Simon, P.; Canizares, A. Raman threshold and rigid to floppy transitions in calcium silicate glasses. *Philos. Mag.* **2005**, *85*, 3357−3378.
(34) Malki, M.; Micoulaut, M.; Chaimbault, F.; Vaills, Y.; Simon, P. Percolative conductivity in alkali earth oxide glasses. *Europhys. Lett.* **2003**, *64*, 661−667.
(35) Micoulaut, M.; Malki, M.; Novita, D. I.; Boolchand, P. Fast ion conduction and flexibility and rigidity of solid electrolyte glasses. *Phys. Rev. B* **2009**, *80*, No. 184205.
(36) Gupta, P. K.; Mauro, J. C. Composition dependence of glass transition temperature and fragility. I. A topological model incorporating temperature-dependent constraints. *J. Chem. Phys.* **2009**, *130*, No. 094503.

(37) Smedskjaer, M.; Mauro, J. C.; Yue, Y. Prediction of glass hardness using temperature-dependent constraint theory. *Phys. Rev. Lett.* **2010**, *105*, No. 115503.
(38) Smedskjaer, M.; Mauro, J. C.; Youngman, R. E.; Hogue, C. L.; Potuzak, M.; Yue, Y. Topological principles of borosilicate glass chemistry. *J. Phys. Chem. B* **2011**, *115*, 12930−12946.
(39) Bauchy, M.; Micoulaut, M. Atomic scale foundation of temperature dependent constraints in glasses and liquids. *J. Non-Cryst. Solids* **2011**, *357*, 2530−2537.
(40) Bauchy, M.; Micoulaut, M.; Celino, M.; Boero, M.; Le Roux, S.; Massobrio, C. Angular rigidity in tetrahedral network glasses with changing composition. *Phys. Rev. B* **2011**, *83*, No. 054201.
(41) Micoulaut, M.; Raty, J. Y.; Otjacques, C.; Bichara, C. Understanding phase-change materials from the viewpoint of Maxwell rigidity. *Phys. Rev. B* **2010**, *81*, No. 174206.
(42) Micoulaut, M.; Kachmar, A.; Bauchy, M.; Le Roux, S.; Massobrio, C.; Boero, M. Structure, topology, rings, vibrational and electronic properties of Ge_xSe_{1-x} glasses across the rigidity transition: A numerical study. *Phys. Rev. B* **2013**, *88*, No. 054203.
(43) Boolchand, P.; Georgiev, D. G.; Qu, T.; Wang, F.; Cai, L.; Chakravarty, S. Nanoscale phase separation effects near r = 2.40 and 2.67, and rigidity transitions in chalcogenide glasses. *C. R. Chim.* **2002**, *5*, 713−719.
(44) Bansal, N. P.; Doremus, R. H. *Handbook of glass properties*; Academic Press: New York, 1986.
(45) Xiang, Y.; Du, J. Effect of strontium substitution on the structure of 45S5 bioglasses. *Chem. Mater.* **2011**, *23*, 2703−2717.
(46) Todorov, I. T.; Smith, W.; Trachenko, K.; Dove, M. T. DLPOLY 3: New dimensions in molecular dynamics simulations via massive parallelism. *J. Mater. Chem.* **2006**, *16*, 1911−1918.
(47) Micoulaut, M.; Le Roux, S.; Massobrio, C. Investigation of size effects on the structure of liquid $GeSe_2$ calculated via first-principles molecular dynamics. *J. Chem. Phys.* **2012**, *136*, No. 224504.
(48) Price, D. L.; Carpenter, J. M. Scattering function of vitreous silica. *J. Non-Cryst. Solids* **1987**, *92*, 153−174.
(49) Du, J.; Corrales, R. First sharp diffraction peak in silicate glasses: Structure and scattering length dependence. *Phys. Rev. B* **2005**, *72*, No. 092201.
(50) Micoulaut, M. Structure of densified germanium dioxide. *J. Phys.: Condens. Matter* **2004**, *16*, L131−L138.
(51) Zhang, M.; Boolchand, P. The Central Role of Broken Bond Bending Constraints in Promoting Glass Formation in the Oxides. *Science* **1994**, *266*, 1355−1356.
(52) Boolchand, P.; Thorpe, M. F. Glass Forming Tendency, Percolation of Rigidity and 1-Fold Coordinated Atoms in Covalent Networks. *Phys. Rev. B* **1994**, *50*, 10366−10369.
(53) Lindemann, F. A. The calculation of molecular vibration frequencies. *Phys. Z.* **1910**, *11*, 609−612.
(54) Bauchy, M.; Qomi, M. J. A.; Bichara, C.; Ulm, F. J.; Pellenq, R. Nanoscale Structure of Cement: the Viewpoint of Rigidity Theory. *J. Phys. Chem. C* **2014**, *118*, 12485−12493.
(55) Mantisi, B.; Tanguy, A.; Kermouche, G.; Barthel, E. Atomistic response of a model silica glass under shear and pressure. *Eur. Phys. J. B* **2012**, *85*, 304.
(56) Wyart, M. On the rigidity of amorphous solids. *Ann. Phys. (Paris, Fr.)* **2005**, *30*, 1−96.
(57) O'Hern, C. S.; Silbert, L. E.; Liu, A. J.; Nagel, S. Jamming at zero temperature and zero applied stress: The epitome of disorder. *Phys. Rev. E* **2003**, *68*, No. 011306.
(58) Berens, P. H.; Mackay, D. H. J.; White, G. M.; Wilson, K. R. Thermodynamics and quantum corrections from molecular dynamics for liquid water. *J. Chem. Phys.* **1983**, *79*, 2375−2389.
(59) Benoit, M.; Kob, W. The vibrational dynamics of vitreous silica: Classical force fields vs. first principles. *Europhys. Lett.* **2002**, *60*, 269−275.
(60) Deschamps, T.; Martinet, C.; Bruneel, J. L.; Champagnon, B. Soda-lime silicate glass under hydrostatic pressure and indentation: A micro-Raman study. *J. Phys.: Condens. Matter* **2011**, *23*, No. 035402.
(61) Neuville, D. R. Viscosity, structure and mixing in (Ca, Na) silicate melts. *Chem. Geol.* **2006**, *229*, 28−42.
(62) Mysen, B. O.; Virgo, D.; Scarfe, C. M. Relations between anionic structure and viscosity of silicate melts—A Raman spectroscopic study at 1 atm and at high pressure. *Am. Mineral.* **1980**, *65*, 690−710.
(63) Xue, X. Y.; Stebbins, J. F.; Kanzaki, M.; McMillan, P. F.; Poe, B. Pressure induced silicon coordination and tetrahedral structural-changes in alkali oxide silica melts up to 12 GPa: NMR, Raman, and infrared-spectroscopy. *Am. Mineral.* **1991**, *76*, 8−26.
(64) Cai, Y.; Thorpe, M. F. Floppy modes in network glasses. *Phys. Rev. B* **1989**, *40*, 10535−10542.
(65) Trachenko, K.; Dove, M. T.; Brazhkin, V. V.; El'kin, F. S. Network rigidity and properties of SiO_2 and GeO_2 glasses under pressure. *Phys. Rev. Lett.* **2004**, *93*, No. 135502.
(66) Kamitakahara, W. A.; Cappelletti, R. L.; Boolchand, P.; Halfpap, B.; Gompf, F.; Neumann, D. A.; Mutka, H. Vibrational densities of states and network rigidity in chalcogenide glasses. *Phys. Rev. B* **1991**, *44*, 94−100.
(67) Newton, M. D.; O'Keeffe, M.; Gibbs, G. V. Ab initio calculation of interatomic force constants in $H_6Si_2O_7$ and the bulk modulus of α quartz and α cristobalite. *Phys. Chem. Miner.* **1980**, *6*, 305−312.
(68) Bauchy, M. Structural, vibrational, and thermal properties of densified silicates: Insights from molecular dynamics. *J. Chem. Phys.* **2012**, *137*, No. 044510.
(69) Benmore, C. J.; Weber, J. K. R.; Wilding, M. C.; Du, J.; Parise, J. B. Temperature-dependent structural heterogeneity in calcium silicate liquids. *Phys. Rev. B* **2010**, *82*, No. 224202.
(70) Mead, R. N.; Mountjoy, G. A molecular dynamics study of densification mechanisms in calcium silicate glasses $CaSi_2O_5$ and $CaSiO_3$ at pressures of 5 and 10 GPa. *J. Chem. Phys.* **2006**, *125*, No. 154501.
(71) Naumis, G. G. Glass transition phenomenology and flexibility: An approach using the energy landscape formalism. *J. Non-Cryst. Solids* **2006**, *352*, 4865−4670.
(72) Arthur, E. P. Chemical composition of window glass. *J. Am. Ceram. Soc.* **1926**, *9*, 204−205.
(73) Cormier, L.; Calas, G.; Cuello, G. J. Structural study of Ca-Mg and K-Mg mixing in silicate glasses by neutron diffraction. *J. Non-Cryst. Solids* **2010**, *356*, 2327−2331.
(74) *Glass Science and Technology*; Uhlmann, D. R., Kreidl, N. J., Eds.; Academic Press: New York, 1986.
(75) Popescu, M. A. *Non-Crystalline Chalcogenides*; Kluwer Academic: New York, 2000.
(76) Tronc, P.; Bensoussan, M.; Brenac, A.; Sebenne, C. Optical-Absorption Edge and Raman Scattering in Ge_xSe_{1-x} Glasses. *Phys. Rev. B* **1973**, *8*, 5947−5956.
(77) Fang, C. Y.; Yinnon, H.; Uhlmann, D. R. A kinetic treatment of glass formation. VIII: Critical cooling rates for Na_2O-SiO_2 and K_2O-SiO_2 glasses. *J. Non-Cryst. Solids* **1983**, *57*, 465−471.
(78) Micoulaut, M. Constrained interactions, rigidity, adaptative networks and their role for the description of silicates. *Am. Mineral.* **2008**, *93*, 1732−1748.
(79) Sharmila, B. H.; Devaraju, J. T.; Asokan, S. A modulated differential scanning calorimetric study of As-Te-In glasses. *J. Non-Cryst. Solids* **2003**, *326−327*, 154−158.
(80) Sreevidya Varma, G.; Das, C.; Asokan, S. Evidence of an intermediate phase in a quaternary Ag bearing telluride glass system using alternatign DSC. *Solid State Commun.* **2014**, *177*, 108−112.
(81) Selvanathan, D.; Bresser, W. J.; Boolchand, P. Stiffness transitions in Si_xSe_{1-x} glasses from Raman scattering and temperature-modulated differential scanning calorimetry. *Phys. Rev. B* **2000**, *61*, 15061−15076.